



Pressure Stabilized Lithium-Aluminum Compounds with Both Superconducting and Superionic Behaviors

Xiaomeng Wang,^{1,2} Yong Wang,¹ Junjie Wang,¹ Shuning Pan,¹ Qing Lu¹,, Hui-Tian Wang,¹ Dingyu Xing,¹ and Jian Sun^{1,*}

¹National Laboratory of Solid State Microstructures, School of Physics and Collaborative Innovation Center of Advanced Microstructures, Nanjing University, Nanjing, 210093, People's Republic of China

²School of Physics and Electronic-Electrical Engineering, Ningxia University, Yinchuan, 750021, People's Republic of China



(Received 7 July 2022; revised 8 October 2022; accepted 8 November 2022; published 9 December 2022)

Superconducting and superionic behaviors have physically intriguing dynamic properties of electrons and ions, respectively, both of which are conceptually important and have great potential for practical applications. Whether these two phenomena can appear in the same system is an interesting and important question. Here, using crystal structure predictions and first-principle calculations combined with machine learning, we identify several stable Li-Al compounds with electride behavior under high pressure, and we find that the electronic density of states of some of the compounds has characteristics of the two-dimensional electron gas. Among them, we estimate that Li₆Al at 150 GPa has a superconducting transition temperature of around 29 K and enters a superionic state at a high temperature and wide pressure range. The diffusion in Li₆Al is found to be affected by an electride and attributed to the atomic collective motion. Our results indicate that alkali metal alloys can be effective platforms to study the abundant physical properties and their manipulation with pressure and temperature.

DOI: [10.1103/PhysRevLett.129.246403](https://doi.org/10.1103/PhysRevLett.129.246403)

The structure and properties of the compounds are usually tied to the valence electrons and orbitals of their ingredient elements [1]. It is well known that pressure has a significant effect on atomic orbitals and chemical bonds, which can induce new physical phenomena and the formation of atypical compounds [2]. Previous works indicate that simple metallic elements demonstrate several intriguing phenomena under extreme conditions [3–11]; for instance, under high pressure, Li [6], Na [7], and Al [8] can form electrides, in which valence electrons localize in the interstitial space as quasi-atoms (ISQs) [12]. Moreover, the electride character plays an important role in the liquid-liquid transition of potassium [9] and the anomalous diffusion of calcium [10]. Besides the above-mentioned elemental systems, a large variety of compounds with electride behavior have been studied [13–16]. For example, Ca₂N is a 2D electride in which electrons are confined in the 2D spaces between the [Ca₂N]⁺ layers [14], and Zhang *et al.* developed a computer-assisted inverse-design method for searching for new inorganic electrides [15].

As the simplest metal in the periodic table, studies have revealed that lithium can form many stable high-pressure compounds, together with other elements, showing various physical and chemical properties. For instance, in dense Li-Be [17] and Li-Cs [18] compounds, novel dimensional reductions of electronic structures to 2D or 1D in 3D crystals were predicted. In addition, the complex formal

oxidation state of lithium in Li-Cs alloys was discussed at different pressures [19,20]. Meanwhile, the potential coexistence of the electride state and superconductivity in the same compound—such as for the representative electride [Ca₂₄Al₂₈O₆]⁴⁺(4e⁻) [13], intermetallic Mn₅Si₃-type Nb₅Ir₃ [16], and the high-pressure lithium compounds CaLi₂ [21,22], Be₂Li [23], Li₆P [24], and Li₆C [25]—has aroused great interest in the conventional superconductor field.

Among the lithium compounds, ambient Li-Al systems were proposed as a possible anode material for solid-state batteries [26], which were investigated theoretically [27–29] and experimentally [30]. For example, in ambient-pressure substoichiometric Li-Al alloys, studies of superionic conduction reveal that Li diffuses via a vacancy-mediated mechanism [28,29], while migration mechanisms in different lithium-ion batteries are quite diverse, including interstitial diffusion, collective motion mechanism, and vacancy mechanism [31]. Despite the intriguing superionic behaviors shown above in the ambient Li-Al compounds, systematic explorations of their high-pressure properties and dynamic behaviors are rare. Recently, a theoretical work found that anomalous bonding in LiAl 1:1 compounds affects the various physical properties, as exemplified by their superconducting transition temperature [32]. However, the dynamic behaviors of particles at two different scales (ions and electrons), superionicity and superconductivity, as well as their emergence at different

temperature ranges in the same system under high pressure, are fascinating and have seldom been discussed.

In this Letter, we predict a series of stable compounds with different stoichiometries in Li-Al systems under the pressure range of 0–150 GPa. Dimensional reductions of electronic structures with significant steplike features near the bottom of the valence band are found in Li_2Al and Li_3Al_2 . Particularly, in the three Li-rich compounds (Li_3Al , Li_4Al , and Li_6Al), both superconducting and superionic behaviors occur in the same system. In addition, with the help of anionlike electron localizations, lithium cations in these Li-rich compounds diffuse with a collective motion mechanism in the superionic states.

Searches for Li-Al alloys with pressures up to 150 GPa are performed using a machine-learning accelerated crystal structure prediction method (MAGUS code) [33,34]. Details of the crystal structure search can be found in the Supplemental Material [35]. The results of the Li-Al binary systems under 50, 100, and 150 GPa with new structures of different stoichiometric ratios are depicted in the convex hull diagrams in Fig. 1(a). The stability of the newly predicted compounds is evaluated by calculating the formation enthalpies with respect to decomposition into the most stable solid phases of Li and Al in the corresponding pressure range. We test the energetic stability of Li-Al by considering zero-point energy (ZPE) and find that its influence is rather small. In addition to the known ambient stoichiometries (LiAl , Li_3Al_2 , and Li_2Al) [25,52,53], our structure searches identify new, thermodynamically stable, Li-rich compounds with stoichiometries of Li_4Al_3 , Li_3Al , Li_4Al , and Li_6Al .

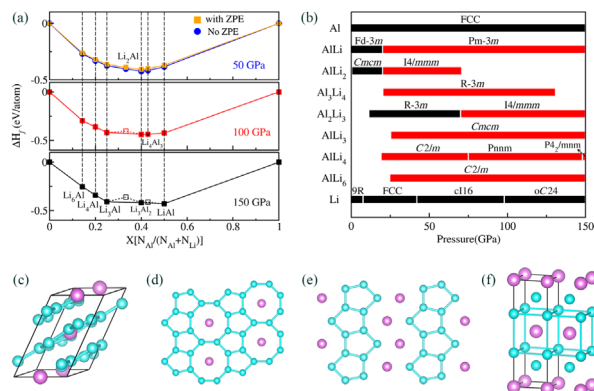


FIG. 1. Energetic stability of the Li-Al system under pressure and structural features of some interesting, stable, high-pressure Li-Al compounds. (a) Calculated convex hulls for the Li-Al compounds at different pressures (50, 100, and 150 GPa). Solid and open symbols represent the thermodynamically stable and metastable compounds. (b) Pressure-composition phase diagram of the Li-Al compounds. (c) Crystal structure of $C2/m$ Li_6Al at 100 GPa. (d,e) Layered feature of the $C2/m$ Li_6Al phase and the $Cmc2$ Li_3Al phase. (f) Crystal structure of $I4/mmm$ Li_2Al at 50 GPa. In these structures, magenta and cyan balls correspond to Al and Li atoms, respectively.

The predicted pressure-composition phase diagram of all structures is summarized in Fig. 1(b). The enthalpy calculations suggest that several compounds may undergo a series of structural phase transitions throughout the pressure range. Phonon dispersion of all the newly predicted compounds is shown in Fig. S2 [35] of the supplemental material, and their lattice dynamical stability is proven by no imaginary frequency. Particularly, phonon calculations (Fig. S2j) clearly show the dynamical stability of $C2/m$ - Li_4Al at 0 GPa, which indicates that once formed at high pressure, this phase might be quenchable to ambient pressure.

The optimized lattice parameters and the atomic positions are summarized in Table SI. As shown in Figs. 1(c)–1(e) and S7–S10, three Li-rich compounds— Li_3Al , Li_4Al , and Li_6Al —have layeredlike geometries, in which structural units of Al and Li atoms are packed on the same plane and then stacked to form 3D structures. The details of each structure are as follows: (i) $Cmc2$ - Li_3Al crystallizes in a quasi-one-dimensional structure, consisting of chains formed by edge-shared, five-membered, lithium rings with channels occupied by Al atoms; (ii) in observation of the single-layer atomic structures of $C2/m$ - Li_4Al , Pnm - Li_4Al , and $P4_2/mnm$ - Li_4Al , it can be seen that each structure contains two pentagons fused together by an edge-sharing Li_8 unit; (iii) for the $C2/m$ - Li_6Al compound, Li atoms construct a 2D sheet with five- and eight-membered rings, and the Al atoms occupy the center of the octagonal ring. The other stable phases with stoichiometries of LiAl , Li_2Al , Li_3Al_2 , and Li_4Al_3 are shown in Figs. 1(f) and S4(a)–S6(a), respectively. The $I4/mmm$ Li_2Al phase and the $I4/mmm$ Li_3Al_2 phase can be viewed as host-guest structures. For $I4/mmm$ Li_2Al , each Al atom sits in the center of a cubic lattice of Li atoms. The $I4/mmm$ Li_3Al_2 phase can be considered as the cubic lattice of Al atoms inserted into the two-layer Li cubic lattice as a guest.

To investigate the electronic properties of these compounds, we calculate the electron localization function (ELF), the difference charge density, electronic band structures, and density of states (DOS). As shown in Fig. 2(a), for the $I4/mmm$ Li_2Al , the DOS at the bottom of the valence band has a striking steplike feature, which suggests a van Hove singularity of a two-dimensional electronic structure. This sharp steplike feature in the DOS usually appears in layered compounds [54], which is quite intriguing, similar to Li-Be alloys [17]. The computed partial charge density for electrons in the energy range specified in the DOS in the inset reveals that the 2D electron gas states are related to the high-electronic-density regions in the layers of Al atoms. This is mainly due to the strong repulsive interaction between the core electrons of Li atoms, which pushes their valence electrons from the Li layer to the Al layer.

Furthermore, the ELF maps of the three Li-rich compounds show that the excess electrons in the interstitial space enclose the Al atoms, forming unique spherical

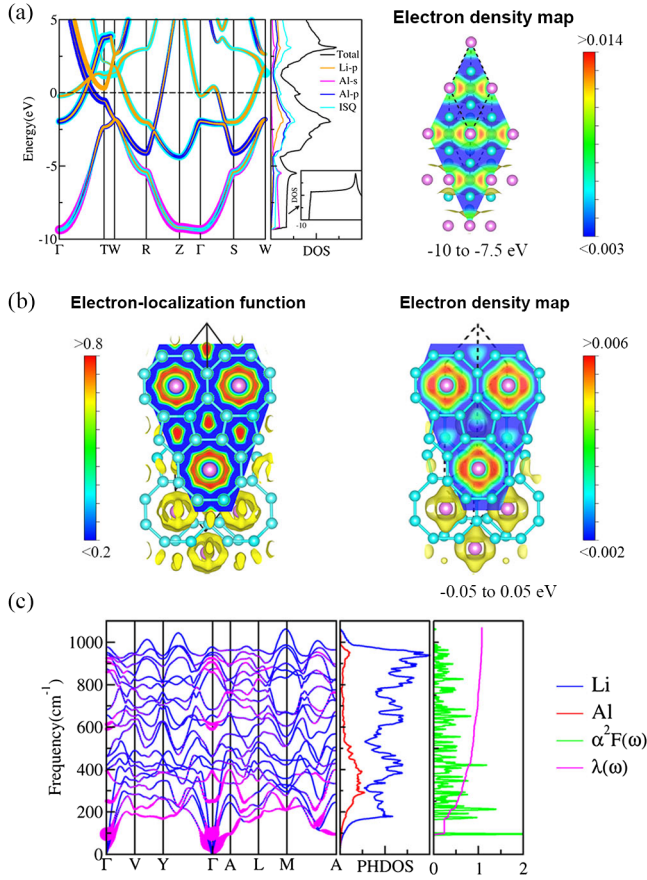


FIG. 2. Electronic properties and superconducting properties of $I4/mmm$ Li_2Al and $C2/m$ Li_6Al . (a) Band structures and PDOS of $I4/mmm$ Li_2Al at 50 GPa. We show electron density maps of the bottom of the valence band ($E = -10$ to -7.5 eV, isosurface of 0.005), which gives the 2D electron gas features in real space. (b) ELF on the $(11-1)$ plane and partial electron density map within an energy ($=50$ meV) corresponding to near the Fermi level of $C2/m$ Li_6Al at 100 GPa. (c) Phonon band structures, projected density of states, Eliashberg spectral function, and electron-phonon coupling constant λ of Li_6Al at 150 GPa. The sizes of the solid violet circles are proportional to the electron-phonon coupling strength.

shell-like electrone states, as seen in Figs. 2(b), S7(c), and S8–S10(c). Furthermore, Bader charge analysis is performed to investigate the charge transfer between Li and Al atoms (Table SII). The results reveal that the charge transfers from Li atoms to Al atoms in Li_3Al , Li_4Al , and Li_6Al are around $2.09e$, $2.78e$, and $4.11e$, respectively, which shows that Al atoms exhibit diverse oxidation values in different systems. The analysis of the band structure shows that these compounds are metallic, with bands crossing the Fermi level (E_F). As shown in Fig. S11(a), Li_6Al exhibits two prominently broadening bands crossing E_F . The partial charge density within an energy ($=50$ meV) corresponding to near E_F reflects that the electrons possess a cross-shaped distribution enclosing Al atoms, which could be considered a feature of s - p orbital

hybridization, as seen in Fig. 2(b). Thus, both the DOS and charge density indicate that the electrical conduction is due to the hybridized states from the Li- s and Al- p orbitals coupled with the orbitals of unique spherical shell-like ISQs.

Since many lithium compounds exhibit superconducting properties under pressure [21–25], we study the potential superconductivity of the new Li-Al alloys. The calculated phonon dispersion and electron-phonon coupling (EPC) constants are depicted in Figs. 2(c), S7, and S10–S11, and Table SIV. We find that the calculated EPC constant λ of $C2/m$ Li_6Al is around 1.08 at 150 GPa, and its superconducting transition temperature (T_c) is estimated to be around 29.0 K (with $\mu^* = 0.1$). To further understand the superconductivity and the effect of pressure on Li_6Al , we plot the phonon dispersion of Li_6Al at 150 GPa and 50 GPa in Figs. 2(c) and S11(c), respectively. Our results can be divided into three parts. (i) Phonon-coupling of Li-Al atoms: From the phonon DOS, one can determine that the low-frequency phonon modes below 300 cm^{-1} are related to the hybridization of the vibrations of Li with Al atoms and give a prominent contribution of around 59.0% to the total λ at 150 GPa. (ii) Phonon softening: It is worth noting that the transverse acoustic modes along the Y- Γ -A directions and the optical mode A_g ($\sim 109\text{ cm}^{-1}$) at the Γ point soften as the pressure increases from 50 to 150 GPa; the large phonon linewidth of these modes implies that they are strongly coupled to the electrons and play a key role in enhancing the superconductivity in Li_6Al compared to the results of low pressures. (iii) In terms of electronic density, we find that when applying high pressure on Li_6Al , the total DOS at E_F increases (Fig. S12), and the shell-like interstitial electron localization surrounding the Al atoms becomes denser (more yellow areas at 150 GPa), which would help phonon vibrations affect more electrons and enhance the electron-phonon coupling, as also shown in those hydrogen-based superconductors [55]. Therefore, with the increase of pressure, the strong enhancement of λ in Li_6Al results from a combined effect of higher electronic DOS and strong-coupling phonon modes, both stemming from hybridization with electronic and vibrational states between Li and Al atoms, as well as the ISQs.

Despite these intriguing dynamic properties of electrons (superconductivity) of the high-pressure Li-Al compounds at low temperatures, these compounds may also possess transport properties at high temperatures in another scale (superionicity) similar to Li-ion battery compounds. Taking Li_6Al at 150 GPa as an example, with *ab initio* and machine-learning molecular dynamics (MLMDs) simulations, we find that, at 800 K, the system demonstrates a solid state [Fig. 3(a)], while at 1600 K, lithium atoms start to diffuse and Al atoms still vibrate at their equilibrium positions, which is the typical superionic behavior [Fig. 3(b)]. Heating to 2000 K, the system shows liquid behavior with random-walk atomic motion [Fig. 3(c)]. Mean square displacements (MSDs) of Li_6Al at different

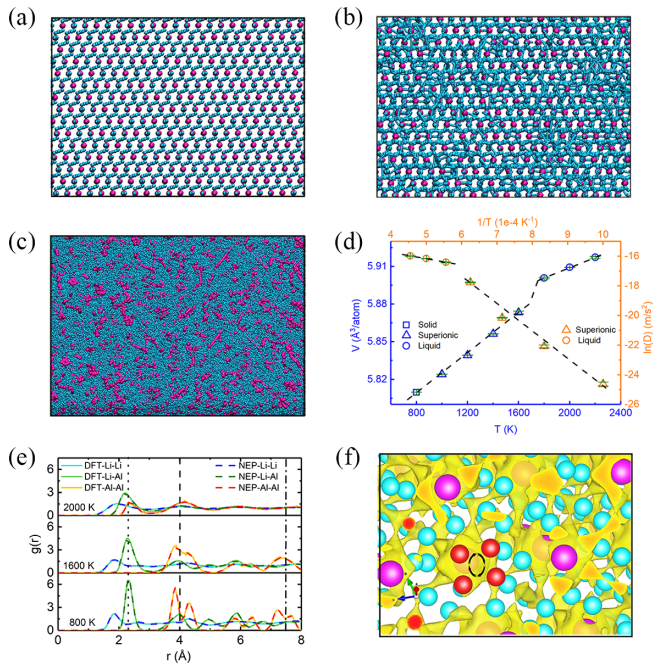


FIG. 3. Finite-temperature thermodynamic behaviors of Li_6Al at different temperatures. (a)–(c), Snapshots extracted from MLMDs at (a) 800 K, (b) 1600 K, and (c) 2000 K, which clearly show the behaviors of solid, superionic, and liquid states. (d) Volume-temperature relationship of Li_6Al at 150 GPa. The discontinuity in volume vs temperature confirms the melting. Diffusion coefficients at different T are displayed via Arrhenius linear regression. Dashed lines are guides to the eye, and green horizontal lines in property symbols are error bars. (e) Radial distribution functions $g(r)$ in solid, superionic, and liquid states. Black vertical lines highlight Li-Li structural short- and long-order changes. (f) Simplest atomic collective diffusion (ring mechanism) with their ELF (0.75) environments, indicating that the superionic state in Li-Al compounds is connected with their electride feature. Four red lithium atoms rotate almost simultaneously above an Al atom that is surrounded by localized electrons.

temperatures also reflect similar phenomena (Fig. S15). The machine-learning potential for Li_6Al is trained on the predicted structures and DFT results of this Letter using the NEP package [56], and this potential is well consistent with DFT results in different aspects, which ensures the robustness of the following results (see details in the Supplemental Material [35]).

Diffusion coefficients in superionic states and liquid can be extracted from MSDs. They satisfy the Arrhenius relation [Fig. 3(d)] and have different activation energies (E_a) for different states (~ 35.13 kJ/mol for the superionic state and ~ 147.76 kJ/mol eV for the liquid). The melting point of Li_6Al at 150 GPa is located at around 1800 K by identifying the volume discontinuity during our MLMD simulations at different T [Fig. 3(d)]. With no structural change for the Al sublattice, the volume change from solid to superionic is slow and continuous, indicating that it is a

type-II superionic matter. Radial distribution functions $g(r)$ [Fig. 3(e)] extracted from MLMD simulations provide us with more transformation details. For instance, at 800 K, $g(r)$ between different atom species indicates both short- and long-range order, while in the 1600 K superionic state, $g(r)$ of Li-Li loses its long-range order and retains some short-range order. In liquid, all $g(r)$ displays typical liquid structural properties and converges to 1 as the radius increases to a large number. We notice that $g(r)$ of Li-Li in the superionic state does not display full liquid behavior, and thus the diffusion behavior is different from the random-walk atomic motion in liquid. Hence, the diffusion mechanism in Li-Al superionic electrides should be elucidated. Previously, tremendous work in Li-ion batteries has revealed different diffusion mechanisms of superionic lithium atoms in solid sublattices [31], including interstitial mechanisms, vacancy mechanisms, and collective motion mechanisms. In our MD simulations, since we use supercells of defect-free Li_6Al single crystals, Li diffusion is directly attributed to atomic collective motion, in which a group of atoms diffuses by pushing its nearest neighbor and hopping to the next equilibrium position to form rings or open loops.

In Fig. 3(f), we show the simplest collective motion in our simulations, in which four atoms rotate to their nearest neighbor almost simultaneously. Previous studies showed that the collective motion of multiple lithium ions could reduce diffusion barriers [57]. More complex atomic collective diffusions in our simulations are shown in the Supplemental Material [35], and we notice that there is a path priority during collective diffusion [Fig. 3(b) and Supplemental Material], which causes the short-range order residual in $g(r)$ for the Li-Li pairs in the superionic state. To understand this priority, electronic structures must be considered. The above results about the electronic structures in this Letter indicate that Li_6Al is a high-pressure electride in which valence electrons of Li are localized interstitially and form a shell-like distribution surrounding the central Al atoms [Fig. 2(b)]. Calculating electronic environments in superionic states, we find that Li does not change its cationic characters at high temperatures since their diffusion only occurs in the open pipes surrounded by an electride. In Fig. 3(f), four-Li-atom ring diffusion rotates in the open space above the shell-like electride. This atomic collective motion assisted by an electride is also identified in high-pressure elemental calcium [10] and has a free energy priority compared to regular random walk diffusions. We believe that similar atomic collective diffusions may occur in other electrides at high-pressure and finite-temperature conditions.

In conjunction with the superconducting properties discussed above, we summarize a temperature-pressure phase diagram of Li_6Al . As shown in Fig. 4, the temperature-dependent phase diagram at high pressure is divided into four distinct regions: the superconducting state, the

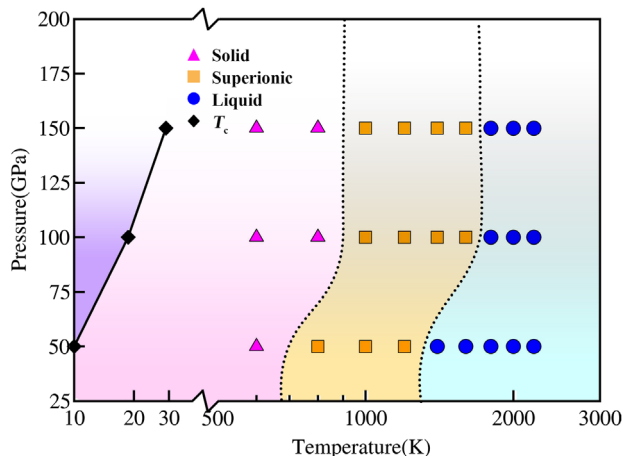


FIG. 4. Proposed temperature-pressure phase diagram of the $C2/m$ Li_6Al . The symbols represent the data points corresponding to four distinct states: triangle, solid state; square, superionic state; circle, liquid state; and diamond, superconducting state. The black dashed lines are the phase boundaries.

solid state, the superionic state, and the liquid state. The superionic region exists over the entire pressure range in which Li_6Al is stable. The superconducting temperature T_c of Li_6Al increases with increasing pressure. The T_c is estimated to be 10.0 K at 50 GPa and 18.7 K at 100 GPa, with a pressure coefficient (dT_c/dP) of 0.19 K/GPa.

In summary, the phase diagram and physical properties of Li-Al systems from 0 to 150 GPa are extensively explored using our crystal structure search method MAGUS and first-principles calculations combined with machine learning. Seven new stable compounds are found. Three pressure-stabilized Li-rich compounds— Li_3Al , Li_4Al , and Li_6Al —are predicted to possess exotic properties. They are high-pressure electrides; in particular, in Li_6Al , some valence electrons localize in the interstitial space to form unique spherical shell-like quasi-atoms and wrap the Al atoms. Interestingly, our calculations show that Li_6Al is a superconductor with a superconducting T_c of 29.0 K at 150 GPa. At high temperatures, superionic states in the Li-rich compounds are identified in a temperature range of a few hundred Kelvin. The diffusion mechanism in defect-free Li_6Al is attributed to atomic collective motion. It is fascinating that we identify both superconducting and superionic states in the same system, reflecting the transport properties of two kinds of particles with very different masses, electrons, and ions. These results are expected to guide future experimental studies on alloys under pressure and help us to understand the collective diffusion in electrides.

J. S. gratefully acknowledges the financial support from the National Key R&D Program of China (Grant No. 2022YFA1403201), the National Natural Science Foundation of China (Grants No. 12125404, No. 11974162, and No. 11834006), and the Fundamental

Research Funds for the Central Universities. The calculations were carried out using supercomputers at the High Performance Computing Center of Collaborative Innovation Center of Advanced Microstructures, the high-performance supercomputing center of Nanjing University.

X. W. and Y. W. contributed equally to this Letter.

*Corresponding author.
jjiansun@nju.edu.cn

- [1] L. Pauling, *The Nature of the Chemical Bond and the Structure of Molecules and Crystals* (Cornell University Press, Ithaca, 1960).
- [2] W. Grochala, R. Hoffmann, J. Feng, and N. W. Ashcroft, The chemical imagination at work in very tight places, *Angew. Chem., Int. Ed.* **46**, 3620 (2007).
- [3] D. U. Gubser and A. W. Webb, High-Pressure Effects on the Superconducting Transition Temperature of Aluminum, *Phys. Rev. Lett.* **35**, 104 (1975).
- [4] K. Shimizu, H. Ishikawa, D. Takao, T. Yagi, and K. Amaya, Superconductivity in compressed lithium at 20 K, *Nature (London)* **419**, 597 (2002).
- [5] V. V. Struzhkin, M. I. Eremets, W. Gan, H.-k. Mao, and R. J. Hemley, Superconductivity in dense lithium, *Science* **298**, 1213 (2002).
- [6] M. Marqués, M. I. McMahon, E. Gregoryanz, M. Hanfland, C. L. Guillaume, C. J. Pickard, G. J. Ackland, and R. J. Nelmes, Crystal Structures of Dense Lithium: A Metal-Semiconductor-Metal Transition, *Phys. Rev. Lett.* **106**, 095502 (2011).
- [7] Y. Ma, M. Eremets, A. R. Oganov, Y. Xie, I. Trojan, S. Medvedev, A. O. Lyakhov, M. Valle, and V. Prakapenka, Transparent dense sodium, *Nature (London)* **458**, 182 (2009).
- [8] C. J. Pickard and R. J. Needs, Aluminium at terapascal pressures, *Nat. Mater.* **9**, 624 (2010).
- [9] H. Zong, V. N. Robinson, A. Hermann, L. Zhao, S. Scandolo, X. Ding, and G. J. Ackland, Free electron to electride transition in dense liquid potassium, *Nat. Phys.* **17**, 955 (2021).
- [10] Y. Wang, J. Wang, A. Hermann, C. Liu, H. Gao, E. Tosatti, H.-T. Wang, D. Xing, and J. Sun, Electronically Driven 1D Cooperative Diffusion in a Simple Cubic Crystal, *Phys. Rev. X* **11**, 011006 (2021).
- [11] M.-S. Miao and R. Hoffmann, High pressure electrides: A predictive chemical and physical theory, *Acc. Chem. Res.* **47**, 1311 (2014).
- [12] J. L. Dye, Electrons as anions, *Science* **301**, 607 (2003).
- [13] M. Miyakawa, S. W. Kim, M. Hirano, Y. Kohama, H. Kawaji, T. Atake, H. Ikegami, K. Kono, and H. Hosono, Superconductivity in an inorganic electride $12\text{CaO}\cdot 7\text{Al}_2\text{O}_3:e^-$, *J. Am. Chem. Soc.* **129**, 7270 (2007).
- [14] K. Lee, S. W. Kim, Y. Toda, S. Matsuishi, and H. Hosono, Dicalcium nitride as a two-dimensional electride with an anionic electron layer, *Nature (London)* **494**, 336 (2013).
- [15] Y. Zhang, H. Wang, Y. Wang, L. Zhang, and Y. Ma, Computer-Assisted Inverse Design of Inorganic Electrides, *Phys. Rev. X* **7**, 011017 (2017).

- [16] Y. Zhang, B. Wang, Z. Xiao, Y. Lu, T. Kamiya, Y. Uwatoko, H. Kageyama, and H. Hosono, Electride and superconductivity behaviors in Mn_5Si_3 -type intermetallics, *npj Quantum Mater.* **2**, 45 (2017).
- [17] J. Feng, R. G. Hennig, N. W. Ashcroft, and R. Hoffmann, Emergent reduction of electronic state dimensionality in dense ordered Li-Be alloys, *Nature (London)* **451**, 445 (2008).
- [18] X. Zhang and A. Zunger, Altered Reactivity and the Emergence of Ionic Metal Ordered Structures in Li-Cs at High Pressures, *Phys. Rev. Lett.* **104**, 245501 (2010).
- [19] J. Botana and M.-S. Miao, Pressure-stabilized lithium caesides with caesium anions beyond the -1 state, *Nat. Commun.* **5**, 4861 (2014).
- [20] S. Desgreniers, J. S. Tse, T. Matsuoka, Y. Ohishi, and J. J. Tse, Mixing unmixables: Unexpected formation of Li-Cs alloys at low pressure, *Sci. Adv.* **1**, e1500669 (2015).
- [21] T. Matsuoka, M. Debessai, J. J. Hamlin, A. K. Gangopadhyay, J. S. Schilling, and K. Shimizu, Pressure-Induced Superconductivity in $CaLi_2$, *Phys. Rev. Lett.* **100**, 197003 (2008).
- [22] Y. Xie, A. R. Oganov, and Y. Ma, Novel High Pressure Structures and Superconductivity of $CaLi_2$, *Phys. Rev. Lett.* **104**, 177005 (2010).
- [23] I. Errea, M. Martinez-Canales, and A. Bergara, Ab initio study of superconducting hexagonal Be_2Li under pressure, *Phys. Rev. B* **78**, 172501 (2008).
- [24] Z. Zhao, S. Zhang, T. Yu, H. Xu, A. Bergara, and G. Yang, Predicted Pressure-Induced Superconducting Transition in Electride Li_6P , *Phys. Rev. Lett.* **122**, 097002 (2019).
- [25] Z. Liu, Q. Zhuang, F. Tian, D. Duan, H. Song, Z. Zhang, F. Li, H. Li, D. Li, and T. Cui, Proposed Superconducting Electride Li_6C by *sp*-Hybridized Cage States at Moderate Pressures, *Phys. Rev. Lett.* **127**, 157002 (2021).
- [26] J. M. Tarascon and M. Armand, Issues and challenges facing rechargeable lithium batteries, *Nature (London)* **414**, 359 (2001).
- [27] X. Q. Guo, R. Podlucky, and A. J. Freeman, Structural and electronic structural properties of ordered LiAl compounds, *Phys. Rev. B* **40**, 2793 (1989).
- [28] A. Van der Ven and G. Ceder, First Principles Calculation of the Interdiffusion Coefficient in Binary Alloys, *Phys. Rev. Lett.* **94**, 045901 (2005).
- [29] C. S. Cucinotta, G. Miceli, P. Raiteri, M. Krack, T. D. Kühne, M. Bernasconi, and M. Parrinello, Superionic Conduction in Substoichiometric LiAl Alloy: An Ab Initio Study, *Phys. Rev. Lett.* **103**, 125901 (2009).
- [30] M. H. Tahmasebi, D. Kramer, R. Mönig, and S. T. Boles, Insights into phase transformations and degradation mechanisms in aluminum anodes for lithium-ion batteries, *J. Electrochem. Soc.* **166**, A5001 (2019).
- [31] L. Yu, X. Zhou, L. Lu, X. Wu, and F. Wang, Recent developments of nanomaterials and nanostructures for high-rate lithium ion batteries, *ChemSusChem* **13**, 5361 (2020).
- [32] C. Li, W. Yang, and H. W. Sheng, Bridge-bond formation in aluminum and its alloys under high pressure, *Phys. Rev. Mater.* **6**, 033601 (2022).
- [33] K. Xia, H. Gao, C. Liu, J. Yuan, J. Sun, H.-T. Wang, and D. Xing, A novel superhard tungsten nitride predicted by machine-learning accelerated crystal structure search, *Sci. Bull.* **63**, 817 (2018).
- [34] H. Gao, J. Wang, Y. Han, and J. Sun, Enhancing crystal structure prediction by decomposition and evolution schemes based on graph theory, *Fundam. Res.* **1**, 466 (2021).
- [35] See Supplemental Material at <http://link.aps.org/supplemental/10.1103/PhysRevLett.129.246403> for more details about methods, phonon spectra, energetics, and charge transfers, which includes Refs. [36–51].
- [36] C. Liu, H. Gao, Y. Wang, R. J. Needs, C. J. Pickard, J. Sun, H.-T. Wang, and D. Xing, Multiple superionic states in helium-water compounds, *Nat. Phys.* **15**, 1065 (2019).
- [37] Q. Gu, D. Xing, and J. Sun, Superconducting single-layer T-graphene and novel synthesis routes, *Chin. Phys. Lett.* **36**, 097401 (2019).
- [38] C. Liu, J. Shi, H. Gao, J. Wang, Y. Han, X. Lu, H.-T. Wang, D. Xing, and J. Sun, Mixed Coordination Silica at Megabar Pressure, *Phys. Rev. Lett.* **126**, 035701 (2021).
- [39] J. P. Perdew, K. Burke, and M. Ernzerhof, Generalized Gradient Approximation Made Simple, *Phys. Rev. Lett.* **77**, 3865 (1996).
- [40] P. E. Blochl, Projector augmented-wave method, *Phys. Rev. B* **50**, 17953 (1994).
- [41] G. Kresse and J. Furthmüller, Efficient iterative schemes for *ab initio* total-energy calculations using a plane-wave basis set, *Phys. Rev. B* **54**, 11169 (1996).
- [42] A. V. Krūkav, O. A. Vydrov, A. F. Izmaylov, and G. E. Scuseria, Influence of the exchange screening parameter on the performance of screened hybrid functionals, *J. Chem. Phys.* **125**, 224106 (2006).
- [43] J. P. Perdew, A. Ruzsinszky, G. I. Csonka, O. A. Vydrov, G. E. Scuseria, L. A. Constantin, X. Zhou, and K. Burke, Restoring the Density-Gradient Expansion for Exchange in Solids and Surfaces, *Phys. Rev. Lett.* **100**, 136406 (2008).
- [44] P. Blaha, K. Schwarz, F. Tran, R. Laskowski, G. K. H. Madsen and L. D. Marks, WIEN2k: An APW+lo program for calculating the properties of solids, *J. Chem. Phys.* **152**, 074101 (2020).
- [45] A. Togo and I. Tanaka, First principles phonon calculations in materials science, *Scr. Mater.* **108**, 1 (2015).
- [46] P. Giannozzi *et al.*, QUANTUM ESPRESSO: A modular and open-source software project for quantum simulations of materials, *J. Phys. Condens. Matter* **21**, 395502 (2009).
- [47] W. L. McMillan, Transition temperature of strong-coupled superconductors, *Phys. Rev.* **167**, 331 (1968).
- [48] P. B. Allen and R. C. Dynes, Transition temperature of strong-coupled superconductors reanalyzed, *Phys. Rev. B* **12**, 905 (1975).
- [49] M. Parrinello and A. Rahman, Crystal Structure and Pair Potentials: A Molecular-Dynamics Study, *Phys. Rev. Lett.* **45**, 1196 (1980).
- [50] G. S. Grest and K. Kremer, Molecular dynamics simulation for polymers in the presence of a heat bath, *Phys. Rev. A* **33**, 3628 (1986).
- [51] A. P. Thompson *et al.*, LAMMPS—A flexible simulation tool for particle-based materials modeling at the atomic, meso, and continuum scales, *Comput. Phys. Commun.* **271**, 108171 (2022).

- [52] K.-F. Tebbe, H. G. Schnering, B. Rüter, and G. Rabeneck, Li_3Al_2 , A new phase in the system Li/Al, *Z. Naturforsch.* **28b**, 600 (1973).
- [53] K. Puhakainen, M. Boström, T.L. Groy, and U. Häussermann, A new phase in the system lithium–aluminum: Characterization of orthorhombic Li_2Al , *J. Solid State Chem.* **183**, 2528 (2010).
- [54] A. N. Kolmogorov and S. Curtarolo, Prediction of different crystal structure phases in metal borides: A lithium monoboride analog to MgB_2 , *Phys. Rev. B* **73**, 180501(R) (2006).
- [55] F. Belli, T. Novoa, J. Contreras-García, and I. Errea, Strong correlation between electronic bonding network and critical temperature in hydrogen-based superconductors, *Nat. Commun.* **12**, 5381 (2021).
- [56] Z. Fan *et al.*, GPUMD: A package for constructing accurate machine-learned potentials and performing highly efficient atomistic simulations, *J. Chem. Phys.* **157**, 114801 (2022).
- [57] X. He, Y. Zhu, and Y. Mo, Origin of fast ion diffusion in super-ionic conductors, *Nat. Commun.* **8**, 15893 (2017).